Chalcogenide Letters Vol. 22, No. 9, September 2025, p. 807 - 820

Fe-doped SnO_2-SnS_2/polypyrrole: an efficient photocatalyst for the degradation of organic pollutant in wastewater

F. Khan [a], S. Noreen [a], M. S. Youssef [b], A. Jilani [c], H. T. Ali [b], G. Mustafa [d], M. Zahid [a,*]

[a] *Department of Chemistry, University of Agriculture, Faisalabad- 38040 Pakistan*

[b] *Department of Mechanical Engineering, College of Engineering, Taif University, Kingdom of Saudi Arabia*

[c] *Clean Energy Technologies Research Institute (CETRI), Process Systems Engineering, Faculty of Engineering & Applied Science, University of Regina, 3737 Wascana Parkway, Regina, Canada*

[d] *Department of Chemistry, University of Okara, Okara Pakistan*

In this study Fe doped SnO_2-SnS_2 (FS) and Fe doped SnO_2-SnS_2-polypyrrole (FS-PPY) were synthesized and studied for the methylene blue (MB) egrdation under UV light. The morphological and structural characterizations were carried out by FTIR, SEM-EDX, XRD and XPS. It has been found that FS-PPy degrade methylene blue upto 98 % under optimized conditions as pH =3, dye concentration = 10 ppm, oxidant dose = 2 mM. The Langmuir-Hinshelwood kinetics model fitted well. The optimization was studied using response surface methodology. Scavengers study was carried out to find the active species. Reusability of photocatalyst was evaluated up to 5 cycles.

(Received June 21, 2025; Accepted September 15, 2025)

Keywords: Fe doped SnO_2-SnS_2, Photocatalysis, UV light, Methylene blue, Characterization, Optimization, Kinetic study

1. Introduction

In modern agricultural and industrial society, several pollutants pass on to the environment and significantly overload air, water and soil. Unusually various pollutants such as pesticides, antibiotics, organic dyes, etc. are carcinogenic and toxic, even very small quantities. If contaminated water is discharged directly into lakes, river and seas without proper treatment it will be harmful towards ecological environment and human health [1]. Dyes are colored organic species that absorbing visible region of light. They are mainly used in paper concrete, plastic medicine, cosmetic printing, rubber, food and textile industry for multiple purposes. Huge amount of wastewater is generated by these industries. Among these, the textile industry utilizes dyes having complex structures. Methylene blue is one of mostly used as coloring agent for paper, cotton, silk and wool. It is a well-known primary thiazine cationic dye [2]. Conventional wastewater treatment methods do not thoroughly degrade methylene blue properly. Thus, effective removal methods have attracted attention widely in industry and academia.

Advanced oxidation process is commonly used for wastewater treatment. This is a robust, effective and low-cost process. Hence, considered as a combative approach for the remediation of organic pollutants. Ozonation, photocatalysis, Fenton, photo-Fenton, electrochemical oxidation and sonolysis are some types of AOPs [3, 4]. Consequently, extensive research studies and development about photocatalysis provide solutions to manage environmental issues. This system involves a photochemical reaction at the surface of semiconductor where two reactions, oxidation and reduction occur simultaneously. Different types of photocatalyst like metal oxides and sulfides have been applied for wastewater treatment.

* Corresponding author: rmzahid@uaf.edu.pk
https://doi.org/10.15251/CL.2025.229.807

SnO_2-SnS_2 has emerged as the leading candidate. As photocatalytic activity is also elevated by forming heterojunction structures. To enhance the light absorbance efficiency surface area and surface reactivity of photocatalyst, the modification of semiconducting material is necessary. Doping with transitions metals like Cu, V, Cr, Mn, Ni, Co and Fe are having been commonly used to enhance the light absorption spectrum of semiconductors [5-7].

Polar and non-porous surface of photocatalyst decrease the sorption of pollutants on its surface. Therefore, immobilization of photocatalyst on supporting material is a favorable strategy. It helps to overcome the main drawback of photocatalyst like agglomeration [8, 9]. Polymer matrices have provided good mechanical strength and stability under different environmental conditions. The polymers like polyvinyle, polythiophene, polyaniline and polypyrrole are used commonly for this purpose. Polypyrrole has been provided due to its ecofriendly nature and stability. It is formed by the polymerization of pyrrole.

The current study focused on FS-PPy composites prepared by the doping of Fe on SnO_2-SnS_2 and its coupling with polypyrole. The composite was used for the eradication of dye from wastewater. The procedure was statistically modeled by response surface methodology to analyze the influence of pH, catalyst dose and oxidant dose. The composite was easily separated from aqueous solution. The recycling efficiency was up to five successive cycles. L-H kinetics was also applied to understand the interaction between photocatalyst and dye.

2. Experimental

2.1. Materials

The chemicals iron (lll) chloride hexahydrate ($FeCl_3.6H_2O$, ≥ 98 %), Sodium hydroxide (NaOH ≥ 98 %) and Tin (lV) chloride pentahydrate ($SnCl_4.5H_2O$ ≥ 98 %) were acquired from Sigma-Aldrich (Germany). Ethanol (C_2H_5OH 92 %) Methanol (CH_3OH 96 %) and Hydrochloric acid (HCl 96 %) from Dae-jung (Korea). The pH of the mixture was regulated using dilute solutions of HCL and NaOH.

2.2. Preparation of Fe doped SnO_2-SnS_2

The Fe doping is done by facile one-pot solvothermal synthesis. In a typical synthesis process $FeCl_3.6H_2O$ was added in 32ml ethanol and 200μL HCl (37%) mixture. The solution was agitated continuously till a transparent solution was obtained. It was then poured into teplon-lined stainless steel autoclave reactor and left for 12 h to procced at 180 °C. After natural cooling to room temperature, the acquired product was centrifuged and wash out thrice using ethanol and distilled water. The sample was dried overnight at 60 °C.

2.3. Preparation of polypyrrole composites

The composite was synthesized by simple polymerization method [10]. 9.6 g f SDS after 5 min sonication and 3g of FS was stirred in 420 ml distilled water at 500 rpm. After 30 min, 3 g of pyrrole was added in drops with constant stirring for 1h. the polymerization was started after mixing a solution of 5.1g APS in 15 ml distilled water by drops while stirring for 2 h. To obtain the precipitates of FS-PPy, the above mixture was put in 400 ml of methanol. Afterward the filtered precipitates were washed several times with distilled water under vacuum till foam formation was stopped. The obtained particles were dried for 12h at 70°C. The schematic diagram for the composite's fabrication is shown in Fig. 1.

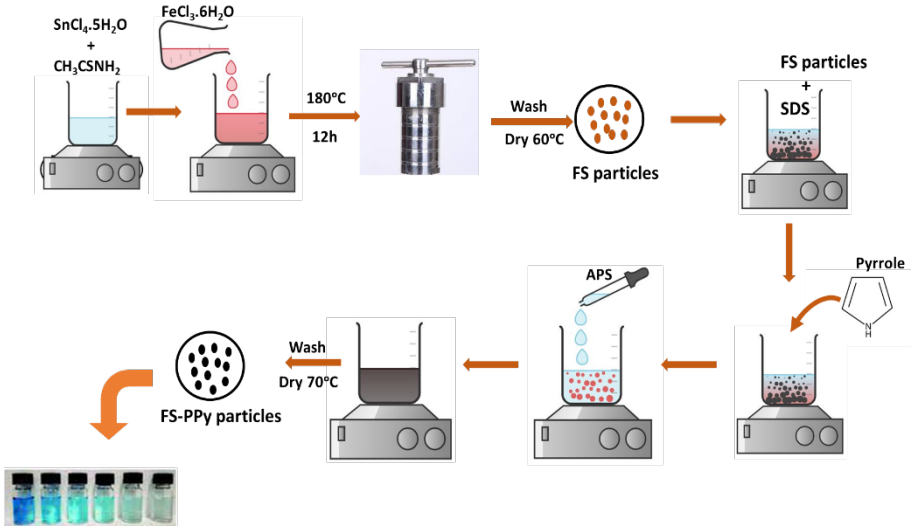

Fig. 1. Illustration of synthesis process of FS and FS-PPy.

2.4. Characterization

The structure of FS and FS-PPy was analyzed by SEM-EDX (SEM JSM-7000 F, ACCEL VOLT 15.0). Functional groups were studied with Fourier transformed infrared (FTIR) spectroscopy. The crystallinity of FS-PPY composite was analyzed by Powder XRD (XRD Ultima-IV: Rigaku, Japan). X-Ray photoelectron spectroscopy (XPS) using Escalab 250 XPS system (Thermo Fisher Scientific UK) was also investigated.

2.5. Photocatalysis experiment

The experiment was done by the addition of photocatalyst in dye containing solution at various physicochemical conditions like pH, photocatalyst dose, oxidant dose, dye concentration and time in UV chamber for 120 min. The photocatalyst (1 mg) was dispersed in MB solution (10 ppm) in a Pyrex beaker at 25 °C. The sample was stirred for 30 min. to stabilize the adsorption-desorption equilibrium. During the UV irradiation, the suspension (3 ml) was taken and centrifuged to take out the photocatalyst. The residual conc. of MB was determined with a UV-Vis spectrophotometer (Cecil 7200, UK) by its characteristic absorption peak located at 664 nm. The degradation capacity is calculated by following formula.

$$\%\ Removal = \left(\frac{C_o - C_t}{C_o}\right) \times 100 \quad (1)$$

C_o and C_t represent the initial and final dye concentrations. The zero charge point of photocatalyst was investigated by solid addition method as described in our previous study [2, 11, 12]

2.6. Detection of reactive species

One of the important themes in the photocatalytic degradation was the detection of reactive species. Different scavengers were added into MB solution prior to the addition of photocatalyst. Such as isopropyl alcohol (IPA), potassium dichromate ($K_2Cr_2O_7$), Ascorbic acid and EDTA. The trapping experiments were executed at optimized condition of samples to study the active species liable for dye degradation [13].

2.7. Polynomial equation-based modeling using response surface methodology

The degradation of MB was studied with central composite design (CCD) based modelling using Design-Expert. Three factors such as pH, photocatalyst dose and oxidant dose were used as variable parameters in CCD model. To attain the optimal conditions a total of 20 experiments were

run. The data was analyzed by multiple regression to fit the quadratic model according to the equation 2.

$$y = b_o + \sum_{i=1}^{n} b_i x_i + \sum_{i=1}^{n} b_{ii} x_i^2 + \sum_{i=1}^{n-1} \sum_{j=i+1}^{n} b_{ij} x_i x_j \quad (2)$$

whereas the predicted response variable y show % degradation of MB. X_i and X_j are coded values for experimental variables. Here, b_i and b_{ii} are linear and is the quadratic coefficients, respectively. b_o is the model constant and b_{ij} is the interaction coefficient. Implication of this equation was confirmed statistically by analysis of variance (ANOVA) [14, 15].

3. Results and discussion

3.1. FTIR analysis of FS and FS-PPy

FTIR has been used to identify the inorganic and organic functional material present in the composite. Fig. 2 depicts the spectrum of FS and FS-PPy from wavenumber ranges 650-4000cm^{-1}. The peak at 2911cm^{-1} is related to C-H stretching (asymmetric). The peak at 1515 cm^{-1} signifies stretching vibration of C=N and asymmetric inter ring C-C vibrations. The peak at 1098 cm^{-1} and 930 cm^{-1} is assigned to stretching vibration of C-N and in plan vibration of N-H appropriately [5, 16, 17]. The C-H stretching vibration was presented by the band between 2800-3000 cm^{-1} [18]. The peaks appeared at 750 cm^{-1} are bond stretching vibrations of Sn-S. The peak close to 2430 cm^{-1} and 2845 cm^{-1} is related to Fe present in the composite [19]. The 662cm^{-1} is the characteristic peak for Sn-O vibration [20]. The peak appear at 1395 cm^{-1} is for deformation vibration of O-H [21].

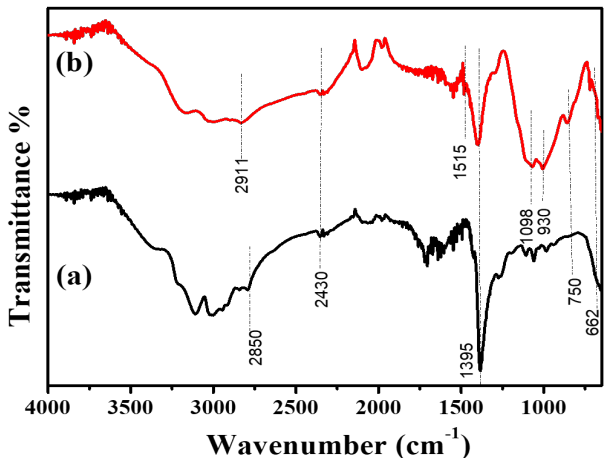

Fig. 2. FTIR spectra of (a) FS and (b) FS-PPY.

3.2. SEM-EDX study

The morphology study and elemental distribution of samples were examined by SEM and EDX. The morphology image in fig. 3 shows the spheroid aggregate structure. This may be due to the high calcination temperature. Compared to pure FS the FS-PPY shows distribution of particles with uniform structure. Which is possibly due to incorporation of FS in new nucleation sites during the polymerization process [22].

The EDX analysis spectrum obtained for FS and FS-PPy confirms the presence of 20.4% O, 18.52% S, 4.53% Fe and 56.51% Sn and 20.13% C, 11.03% O, 9.76 % N, 17.32% S, 2.30% Fe, 39.46% Sn by weight in the composite material respectively [23].

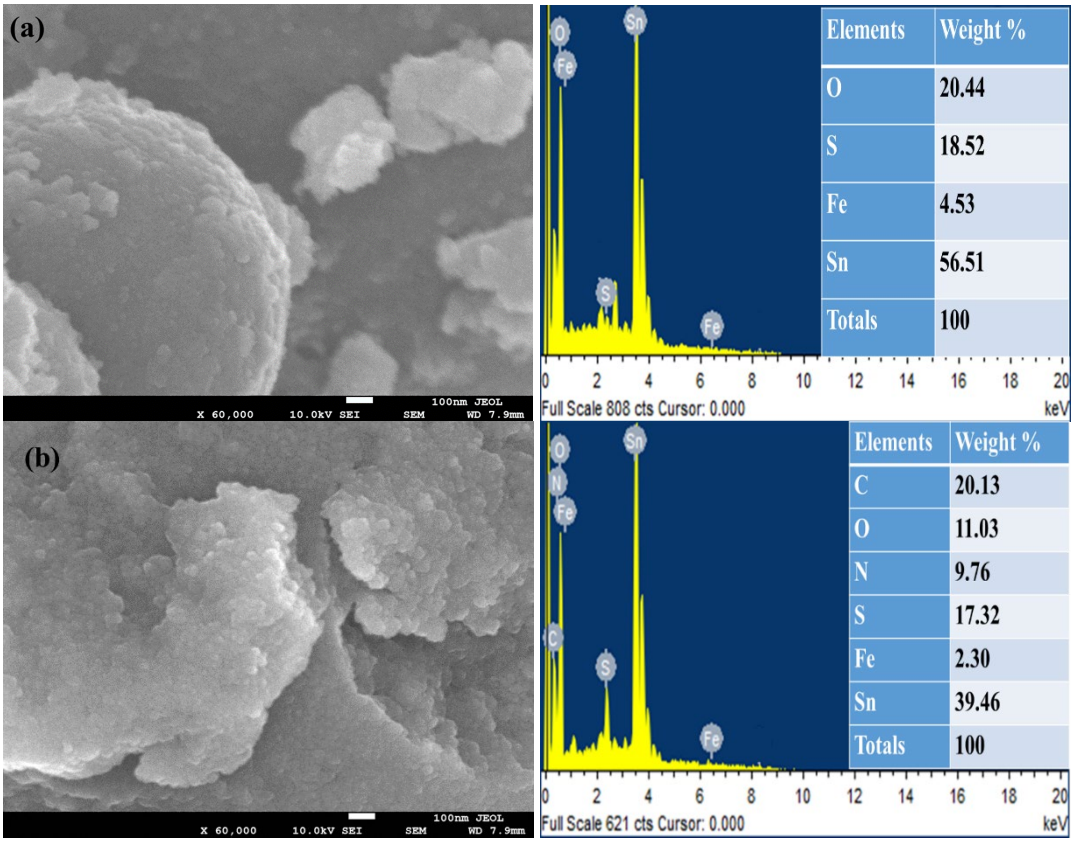

Fig. 3. SEM images and EDX analysis of FS and FS-PPY.

3.3. XRD study

The XRD pattern for FS and FS-Ppy is illustrated in fig. The obtained results show that existence of Fe containing compounds have not been noticed. However, Fe dopant amount had increased the intensity of diffraction peaks. The diffraction pattern shows peaks for SnS_2 (JCPDS card no. 23-0677) at 28.4, 32.3, 50.4 and 52.7° corresponds to (100), (101), (110) and (111) respectively [24]. The diffraction peaks perfectly corresponds to rutile SnO_2 (JCPDS card no. 41-1445) showing high crystalline structure obtain through hydrothermal process.[25]. The peaks appeared at 26.9, 34.11, 37.09, 51.01, 54.3, 62.4, 65.6, 66.1, 71.3, 75.8 and 78.9° can be indexed to the lattice plane of (110), (101), (200), (211), (220), (002), (310), (112), (301), (202), (321) and (330), respectively. Fe incorporation to SnO_2-SnS_2. The acquired results clearly indicate that grain progress of SnO_2-SnS_2 was managed by Fe. The diffraction peaks moderately shifted towards wider angle upon doping. This is due to the lower ionic radii of Fe (Fe^{2+} 76 pm and Fe^{3+} 65 pm) as compared to Sn (Sn 140 pm and Sn $^{2+}$ 118 pm). It indicates that Fe integration induces strain and lattice distortion in the crystal matrix of SnO_2-SnS_2 hence persuade some changes in crystal parameters.[26-28]

The average crystallite size was estimated with Debye-Scherrer formula.

$$D = \frac{K\lambda}{\beta\cos\theta} \tag{3}$$

where D is the thickness. K is dependent constant, λ is wavelength, and β is full width half maximum [29]. The particle size is calculated to be 48 nm and 33.4 nm for FS and FS-PPY respectively.

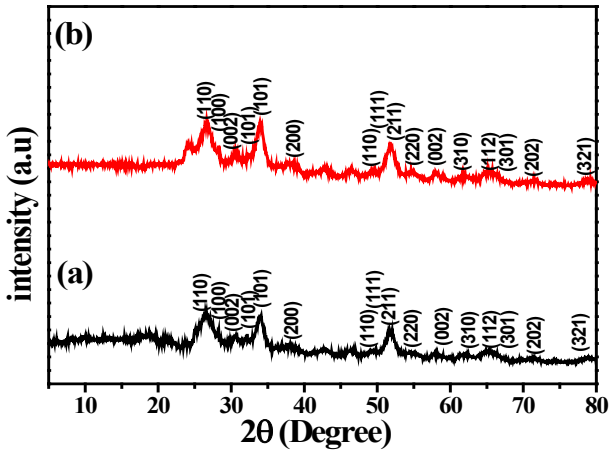

Fig. 4. XRD spectra of (a) FS and (b) FS-PPY.

3.4. XPS analysis of FS and FS-PPy

The valence states and elemental composition were determined by XPS. Fig. 5. approves the existence of all constituents' elements in the photocatalyst. In Fig. 5(A), the two peaks at 980 eV and 532 eV corresponds to hydroxyl and lattice O of SnO_2 [30]. For Fe LMM, Fe LMM1 and Fe LMM2 peaks are centered at 770, 845, 890 eV confirm the metallic state of Fe in SnO_2-SnS_2 particles [9, 31]. 760, 725, 500, 495 and 25 eV are comparable to the recorded peaks of Sn3p1, Sn 2p3, Sn 3d3, Sn 3d5 and Sn 4d [32]. After polymerization the peaks at 405 eV for Ns1 and 290 eV for C1s show that the process is successful. The quantitative data supports this in survey scan.

In fig. 5(B) reports the % atomic composition of Fe doped and PPY modified sample surfaces. The polymerization provides greater extent of C and N along with all other elements [33].

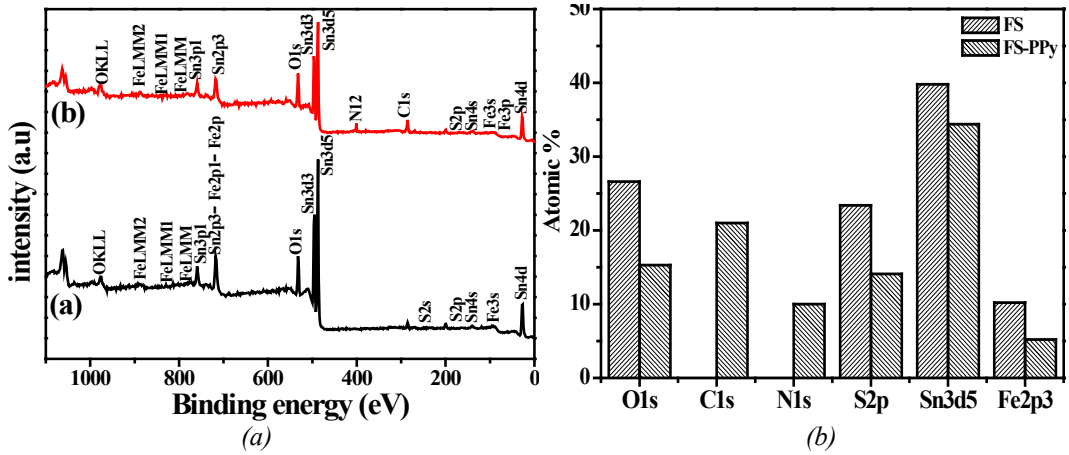

(a) *(b)*

Fig. 5. (A) XPS spectra of (a) FS and (b) FS-PPY and (B) survey scan.

4. Influencing parameters

The MB degradation experiments were performed to investigate the photocatalytic functioning of as-fabricated composites. While studying one parameter, other parameters were kept constant.

4.1. Effect of pH

The dye degradation was investigated at various pH values from 2-9 has been shown in Fig. 6(a). It has been observed that dye degrading efficiency for FSPPY increased in acidic environment as compared to basic conditions. The percentage dye degradation was found to be 92% for FS-PPy at pH 2 and 80 % for FS at pH 8. Generally, pH value effects the electrostatic interaction between pollutant and charged particles that affect the rate of sorption on the surface of composite material. Consequently, optimum pH confirmed for specified photocatalyst. pH_{zc} is the major influencing factor of adsorption. As acidic and basic conditions lead to formation of protonated and deprotonated catalyst surface. The zero charge point pH_{zc} was estimated by solid addition method [34].

4.2. Effect of catalyst dose

The dose of FS and FS-PPy varied from 2-40 mg as presented in Fig. 6(b). It was observed that with increasing the quantity of photocatalyst the degradation of dye was also increasing. However, when the amount of photocatalyst reach the optimal amount, 20 mg for FS and 30 mg for FS-PPy, there is a decline in photodegradation value. It is because of the decreasing available active sites for sorption and catalysis.

4.3. Effect of dye concentration

The dye concentration affect was investigated by changing the concentration from 2-20 ppm with optimized amount of catalyst dose and pH. It has been noticed in Fig. 6(c) that percentage degradation of dye gradually increases by elevating the dye initial concentration. The percentage of degradation was 98 % for 10 ppm dye concentration. Further increasing dye concentration decreases the degradation efficiency. This may be related to the fixed amount of photocatalyst present in the reaction medium. As was expected, there is a specific number of active sites for dye degradation. At high concentration of MB, there will be numerous dye molecules and intermediate that will compete for oxidative species. Furthermore, dye molecules remain non dissociated at high concentration. Thus, it determines the oxidation reaction as rate limiting step.

4.4. Effect of oxidant dose

Addition of external oxidant like H_2O_2 into photocatalyst suspended dye solution raise the degradation efficacy. Recombination of electron-hole pair can be prevented with more electron acceptor in photocatalyst as they increase a multitude of trapped electrons. Moreover, high number of oxidizing species generate reactive radicle in photocatalytic activity thus improve the degradation of intermediate molecules. Excessive amount of oxidant decreases the rate of reaction as shown in Fig. 6(d).

4.5. Effect of time

The percentage of photodegradation versus time is shown in Fig. 6(e). The effect of time was examined from 10 to 120 min. It shows that catalyst efficiency increases with increasing time. The percentage degradation generally improves by increasing time up to 70 min with no significant enhancement thereafter. At the beginning of the process, several available active sites on the surface of photocatalyst, leading to speed up adsorption followed by degradation. As the reaction continued, the active sites steadily occupied so their availability for dye molecules was not sufficient. Thus, degradation rate slows down until a pore diffusion stage reaches. It was a rate determining step [35].

4.6. Kinetics study of photocatalytic degradation

Fig. 6(f) shows the MB degradation and the corresponding kinetics. The linear plot between ln C_o/C and time (t) demonstrates that MB degradation follows L-H kinetics.

$$ln\frac{C_o}{C} = k_{app}t \tag{4}$$

whereas C_o/C is normalized concentration. The parameter k is apparent rate constant (min^{-1}) [36-38]. When MB initial concentration was 10 ppm, the highest degradation rate was investigated. And the apparent rate constant was attained with the value 0.0332 min^{-1} and R^2 is 0.97.

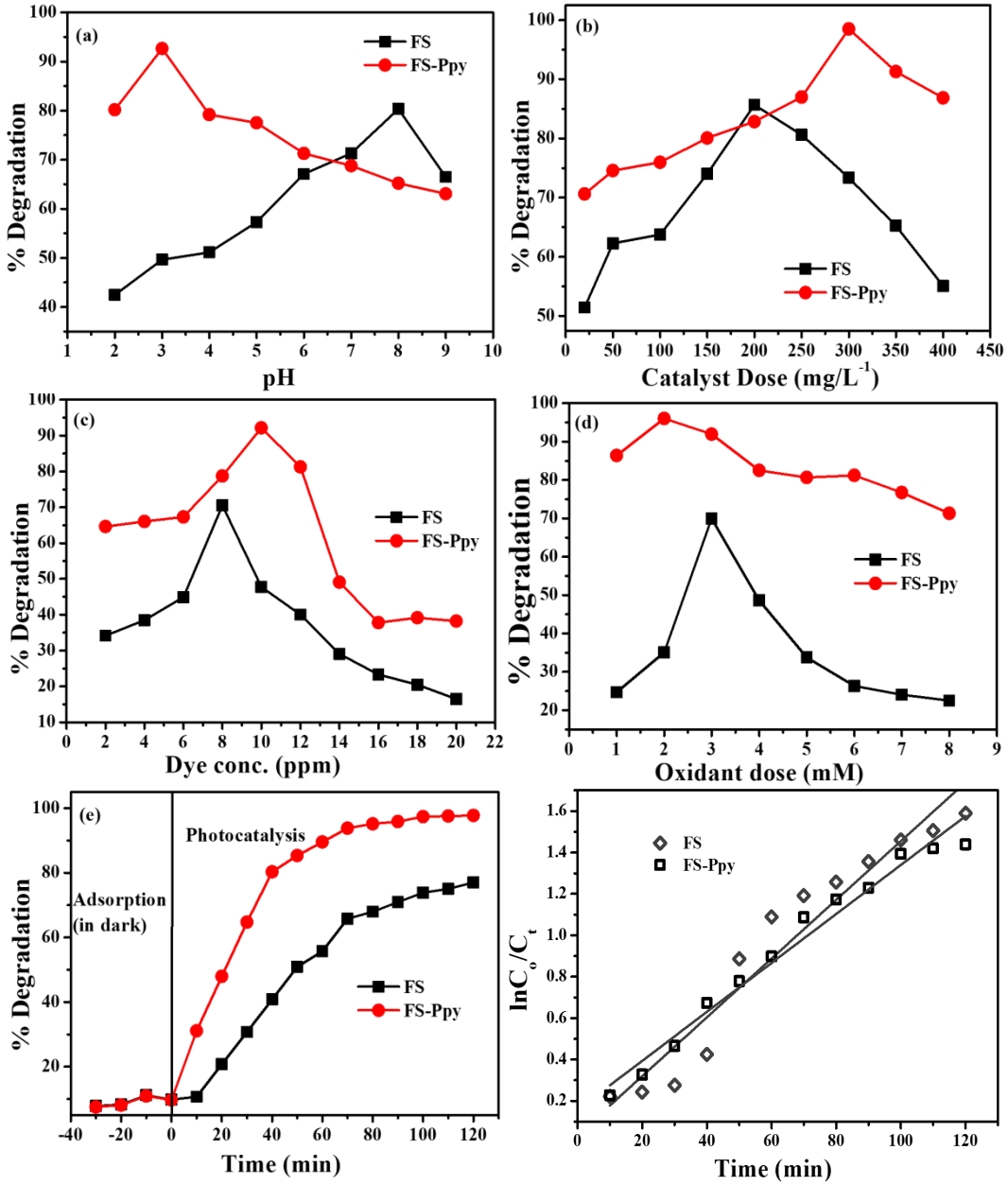

Fig. 6. Influential parameters (a) pH, (b) Catalyst dose, (c) conc. of dye, (d) oxidant dose, (e) irradiation time and (f) L-H kinetics for FS and Fs-PPy.

4.7. Reusability

To test the photocatalyst stability and reusability of FS-PPY five rounds of cycling experiment were done. Each cycle comprises 30 min of dark adsorption and 120 min of UV light irradiation. The photocatalyst does in each cycle was fixed at 30mg for FSPPY and 20 mg for FS. 100ml of 10ppm MB solution was used. After every cycle the composite material was separated by filtration and centrifugation. Wash away with distilled water and ethanol three times than dried at 90 °C for 12h. Because there was some loss of photocatalyst during the regular process of MB degradation. The five-cycle photocatalytic performance of FS-PPY is shown in Fig. 7(a). It shows

an insignificant slowdown with an increasing number of cycles. At the end of the fifth cycle the photodegradation rate still reached 58 % for FS and 76 % for FS-PPy. The slightly decreasing efficiency was mainly caused by the deposition of MB at active sites on the surface of photocatalyst [39-41].

4.8. Effect of scavengers and mechanism of photocatalytic activity

The radical scavenging study on photocatalytic degradation was studied using different scavengers and results are depicted in Fig. 7(b). Based on trapping experimental results, $O_2^{\bullet-}$ is the main active species during photocatalysis. As MB attached on the surface of photocatalyst, it injects its electrons into CB of semiconductor forming $OH^{\bullet}$ and$O_2^{\bullet}$. The reactive oxygen species attack electrophilically on positive carbon radicals of the dye. The byproducts are formed as low molecular weight organic matter [42]. Fig. 7(c) shows the proposed mechanism in UV light irradiation. The valence band electrons of both semiconductor and polymer excited and transferred to conduction band and holes left behind. These photogenerated charged species rapidly tend to recombine consequently lowers the photocatalytic performance. The most significant function of transition metal dopant (Fe) is acting as an electron-hole trap. It plays a crucial role during the heterojunction system. The charge carriers trapping can reduce the recombination (electron-hole) rate and subsequently, increase the life period of charge carriers. When polypyrrol is prepared by oxidative polymerization to contain free electrons on long chain of polymer. The combination of free electrons with oxygen form superoxide radicles.

$$Fe/SnO_2\text{-}SnS_2/PPy + h\upsilon \rightarrow Fe/\ SnO_2\text{-}SnS_2^{*}\ (e^- + h^+),\ PPy\ (e^- + h^+) \quad (5)$$

$$O_2 + e^- \rightarrow O_2^{\bullet-} \quad (6)$$

$$OH^- + h^+ \rightarrow OH^{\bullet} \quad (7)$$

$$H_2O_2 + O_2^{\bullet-} \rightarrow OH^- + OH^{\bullet} + O_2 \quad (8)$$

$$\text{Dye (MB)} + OH^{\bullet} \rightarrow \text{harmless products} \quad (9)$$

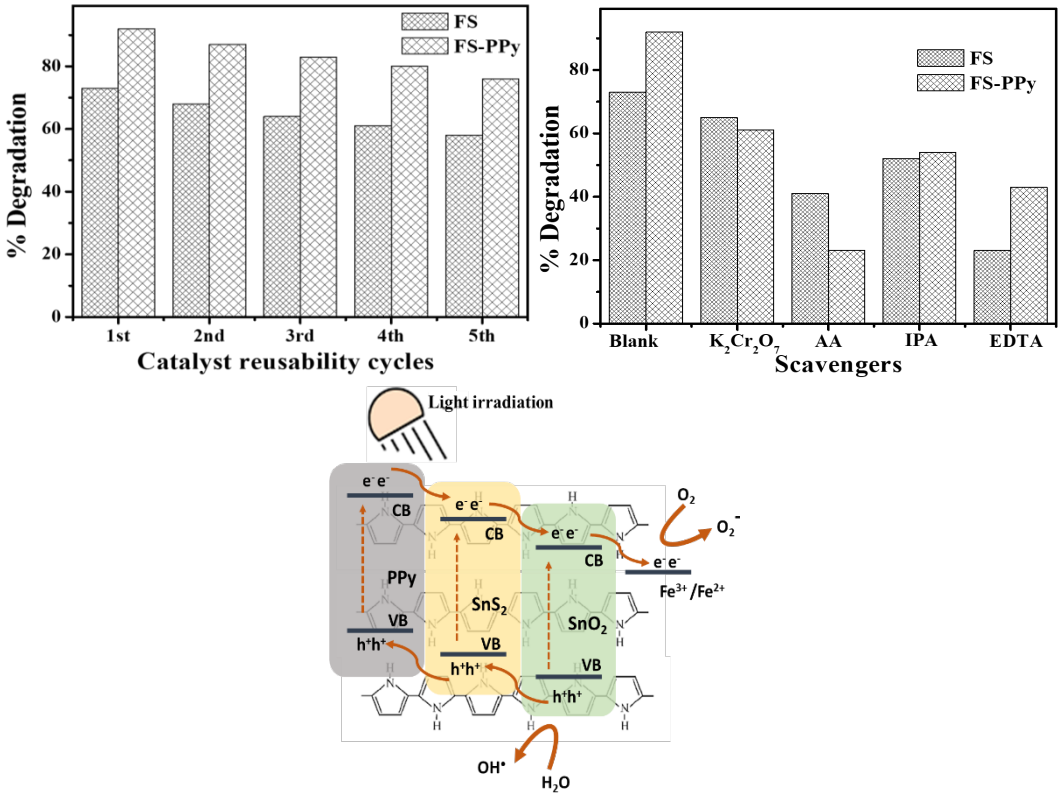

Fig. 7. (a) Photocatalyst reusability, (b) effect of scavengers and (c) proposed mechanism for the photocatalytic degradation.

5. Response surface methodology (RSM)

In this study three treatment factors as, independent variables were evaluated. These were pH, photocatalyst dose and oxidant dose showing relevant influence on dependent variable was percentage (%) degradation. The range and levels of treatment factors were shown in table 1. Sets of twenty experiments were measured including 2^3 factorial experiments, 6 axial points estimating second order model and 6 replicates of center points determine curvature of response surface. The center points devised all variables at zero level. While combination of variables consisting of one at lower and other at higher level [43-45].

Table 1. Real and coded experimental and independent variables for MB degradation.

Variables	Coding	unit	Levels				
			-α	-1	0	+1	α
pH	A		1	2	3	4	5
Photocatalyst dose	B	mg/100ml	20	25	30	35	40
Oxidant dose	C	mM	0	1	2	3	4

Table 2. Analysis of variance for MB degradation.

Source	**Sum of Squares**	**Df**	**Mean Square**	**F Value**	**p-value Prob >F**	**Remarks**
Model	7308.86	9	812.10	7.96	0.0016	significant
A-pH	45.43	1	45.43	0.45	0.5197	
B-Photocatalyst (mg/100ml)	842.60	1	842.60	8.26	0.0166	
C-Oxident dose (mM)	207.80	1	207.80	2.04	0.1840	
AB	392.00	1	392.00	3.84	0.0784	
AC	112.50	1	112.50	1.10	0.3184	
BC	200.00	1	200.00	1.96	0.1917	
A^2	1035.45	1	1035.45	10.15	0.0097	
B^2	2878.65	1	2878.65	28.22	0.0003	
C^2	2597.81	1	2597.81	25.47	0.0005	
Residual	1020.14	10	102.01			
Lack of Fit	1020.14	5	204.03			
Pure Error	0.000	5	0.000			
Cor Total	8329.00	19				
Std. Dev.	10.10	R-Squared	0.8775			
Mean	72.50	Adj R-Squared	0.7673			
C.V. %	13.93	Pred R-Squared	0.0456			
PRESS	7949.46	Adeq Precision	9.152			

The equation is obtianed as:

$$\% \text{ Degradation} = +97.11 - 1.82 A + 7.85 B + 3.90 C + 7.00 A B + 3.75 A C - 5.00 B C - 8.48 A^2 - 14.13 B^2 - 13.43 C^2$$

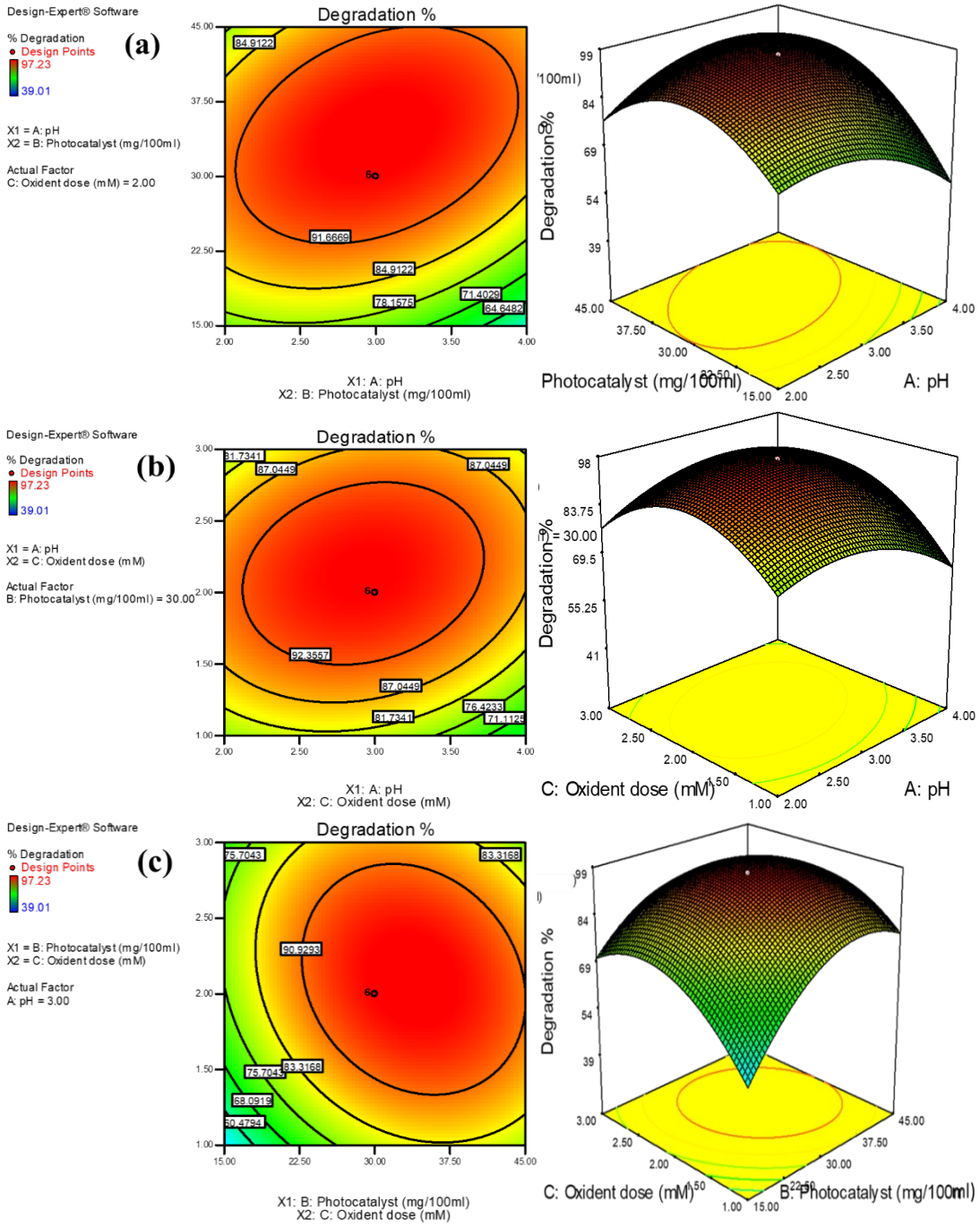

Fig. 8. Show contour and three dimensional plot for interaction effect between two selected veriables.

6. Conclusion

SnO_2-SnS_2 was fabricated via hydrothermal synthesis. FS-PPY was prepared by facile one-pot solvothermal method followed by in situ polymerization of polypyrrole. SEM analysis clearly shows the FS-PPy smaller structure. XRD pattern confirmed that. effect of influencing parameters shows up to 98 % degradation for MB. FS-PPy show a significantly higher efficiency as compared to FS. At pH 2 the degradation was highest to 98 %. Using RSM the optimal conditions were found. The FS-PPY shows excellent efficiency for MB removal.

The superior photocatalytic performance of FS-PPY was due to more efficient transfer of photogenerated charged species. In addition, the process of high rate of adsorption followed by

degradation results from the synergistic effects of three components in FS-PPY. Radical trapping experiment suggested that MB was mainly degraded by superoxide radical ($O_2^{\bullet-}$). Thus, helpfully this work will provide a well-established procedure for the research and development of new photocatalysts as FS-PPY is useful for preparing novel ternary photocatalyst with higher activities.

Acknowledgments

The authors would like to acknowledge Deanship of Graduate Studies and Scientific Research, Taif University for funding this work.

References

[1] J. Li, Y. Ding, K. Chen, Z. Li, H. Yang, S. Yue, Y. Tang, Q. Wang, Journal of Alloys Compounds 903 163795(2022); https://doi.org/10.1016/j.jallcom.2022.163795
[2] I. Khan, K. Saeed, I. Zekker, B. Zhang, A. H. Hendi, A. Ahmad, S. Ahmad, N. Zada, H. Ahmad, L. A. Shah., Water 14 242(2022); https://doi.org/10.3390/w14020242
[3] D. Kanakaraju, B. D. Glass, M. Oelgemöller, Journal of environmental management 219 189-207(2018); https://doi.org/10.1016/j.jenvman.2018.04.103
[4] J.A. Garrido-Cardenas, B. Esteban-García, A. Agüera, J. A. Sánchez-Pérez and F. Manzano-Agugliaro, International Journal of Environmental Research and Public Health 17 170(2020); https://doi.org/10.3390/ijerph17010170
[5] Y. Zhang, H. Dong, W. Du, C. Dong, M. Xiong, N. Yang, S. Zhao, H. He, Z. Nie, Chemical Engineering Journal 505 159419(2025); https://doi.org/10.1016/j.cej.2025.159419
[6] Q. Xiong, Z. Yuan, Y. Zhang, Z. Chen, K. Wei, W. Ma, Solar Energy 299 113810(2025); https://doi.org/10.1016/j.solener.2025.113810
[7] Z.K. Heiba, N.M. Farag, M.B. Mohamed, A. Badawi, ECS Journal of Solid State Science and Technology 14 026004(2025); https://doi.org/10.1149/2162-8777/adb17d
[8] D. Yu, H. Peng, C. Yu, W. Ji, X. Wang, S. Pu, Journal of Earth Science 36 1226-1235(2025); https://doi.org/10.1007/s12583-024-0119-8
[9] Q. Jiang, Y. Ma, P. Zhao, X. Li, Y. Shao, X. Xu, Environmental Science & Technology 59 14182-14192(2025); https://doi.org/10.1021/acs.est.5c06061
[10] D.A. González-Casamachin, J.R. De la Rosa, C.J. Lucio-Ortiz, D.A.D.H. De Rio, D.X. Martínez-Vargas, G.A. Flores-Escamilla, N.E.D. Guzman, V.M. Ovando-Medina, E. Moctezuma-Velazquez, Chemical Engineering Journal 373 325-337(2019), https://doi.org/10.1016/j.cej.2019.05.032
[11] Y. Slimani, Z. H. Al Naji, E. Hannachi, M. Nawaz, R. Sivakumar, S. Akhtar, M. A. Almessiere, A. Baykal, R. Vignesh, A. Thakur, Inorganic Chemistry Communications 159 111803(2024); https://doi.org/10.1016/j.inoche.2023.111803
[12] N. Tajat, W. El Mouhri, W. El Hayaoui, I. Nadif, A. Idlahcen, I. Bakas, M. Badreddine, M. Tamimi, A. Assabbane, S. Qourzal, Colloids and Surfaces A: Physicochemical and Engineering Aspects 681 132789(2024); https://doi.org/10.1016/j.colsurfa.2023.132789
[13] V. Gadore, A. K. Singh, S. R. Mishra, M. D. Ahmaruzzaman, Scientific Reports 14 1-20(2024); https://doi.org/10.1038/s41598-024-51618-2
[14] M. Esfandiaribayat, M. Binazadeh, S. Sabbaghi, M. Mohammadi, S. Ghaedi, H. Rajabi, Scientific reports 14 1163(2024); https://doi.org/10.1038/s41598-024-51847-5
[15] E.a.A.N.-E. Shabanian-Boroujeni, Journal of Photochemistry and Photobiology A: Chemistry 446 115148(2024); https://doi.org/10.1016/j.jphotochem.2023.115148
[16] L. Cui, J. Shen, F. Cheng, Z. Tao, J. Chen, Journal of Power Sources 196 2195-2201(2011); https://doi.org/10.1016/j.jpowsour.2010.09.075
[17] I. Šeděnková, O. Taboubi, M. Paúrová, J. Hromádková, M. Babič, Synthetic Metals 292 117218(2023); https://doi.org/10.1016/j.synthmet.2022.117218
[18] G.T. Rao, B. Babu, R. V. S. S. N. Ravikumar, J. Shim, C. V. Reddy, Materials Research Express 4 125021(2017); https://doi.org/10.1088/2053-1591/aa9de5

[19] A.a.M.B. Javed, Journal of Alloys and Compounds 759 14-21(2018); https://doi.org/10.1016/j.jallcom.2018.05.158
[20] S.S. Sana, A. Pasha, D. V. Kumbhakar, S. C. Pawar, H. Li, T. Hou, M. Sharma, V. J. Gupta, Z. Zhang, Nano-Structures and Nano-Objects 33 100918(2023); https://doi.org/10.1016/j.nanoso.2022.100918
[21] D. Toloman, A. Popa, M. Stan, C. Socaci, A. R. Biris, G. Katona, F. Tudorache, I. Petrila F. Iacomi, Applied Surface Science 402 410-417(2017); https://doi.org/10.1016/j.apsusc.2017.01.064
[22] C. Aydin, Journal of Materials Science: Materials in Electronics 29 20087-20096(2018); https://doi.org/10.1007/s10854-018-0140-8
[23] X. Sun, Z. Liu, J. Guo, H. Li, D. Wei, Z. Li, N. Zhou, T. Zhao, G. Yu, Y. Li, Journal of Physics Chemistry of Solids 146 109572(2020); https://doi.org/10.1016/j.jpcs.2020.109572
[24] Z. Yan, J. Chen, X. Huang, X. Zhu, Journal of Materials Science: Materials in Electronics 32 23363-23370(2021); https://doi.org/10.1007/s10854-021-06822-5
[25] W.B.H. Othmen, B. Sieber, H. Elhouichet, A. Addad, B. Gelloz, M. Moreau, S. Szunerits, R. Boukherroub, Materials Science in Semiconductor Processing 77 31-39(2018); https://doi.org/10.1016/j.mssp.2017.12.014
[26] A.A.B. Baig, V. Rathinam, V. Ramya, Materials Technology 36 623-635(2021); https://doi.org/10.1080/10667857.2020.1786781
[27] W.B.H. Othmen, Z. B. Hamed, B. Sieber, A. Addad, H. Elhouichet, R. Boukherroub, Applied Surface Science 434 879-890(2018); https://doi.org/10.1016/j.apsusc.2017.11.019
[28] X. Zhao, T. Wen, J. Zhang, J. Ye, Z. Ma, H. Yuan, X. Ye, Y. Wang, RSC advances 7 21678-21685(2017); https://doi.org/10.1039/C7RA01655G
[29] A.G. Habte, F. G. Hone, F. B. Dejene, Journal of Nanomaterials 2022 (2022); https://doi.org/10.1155/2022/5957125
[30] L. Liu, Y. Wang, K. Guan, Y. Liu, Y. Li, F. Sun, X. Wang, C. Zhang, S. Feng, T. Zhang, Sensors and Actuators B: Chemical 393 134252(2023); https://doi.org/10.1016/j.snb.2023.134252
[31] S. Pan, S. Bera, S. Sen, A. Das, Inorganic Chemistry Communications 152 110672(2023); https://doi.org/10.1016/j.inoche.2023.110672
[32] X. Kou, F. Meng, K. Chen, T. Wang, P. Sun, F. Liu, X. Yan, Y. Sun, F. Liu, K. Shimanoe, Sensors and Actuators B: Chemical 320 128292(2020); https://doi.org/10.1016/j.snb.2020.128292
[33] K. Jlassi, M. H. Sliem, F. M. Benslimane, N. O. Eltai, A. M. Abdullah, Progress in Organic Coatings 149 105918(2020); https://doi.org/10.1016/j.porgcoat.2020.105918
[34] F. Naz, G. A. K. Nabi, A. Nawaz, S. Ali, M. Siddique, Journal of Cluster Science (2023).
[35] Y. Wang, L. He, G. Dang, H. Li, X. Li, Journal of Colloid and Interface Science 592 51-65(2021); https://doi.org/10.1016/j.jcis.2021.02.033
[36] R.D. Alli, N. Ghafarvand, M. H. Sedghkerdar, N. Mahinpey, Journal of the Energy Institute 118 101898(2025); https://doi.org/10.1016/j.joei.2024.101898
[37] T. Wang, J. Li, L. Shi, X. Dai, Journal of Environmental Chemical Engineering 13 115393(2025); https://doi.org/10.1016/j.jece.2025.115393
[38] D. Zhou, C. Dang, X. Chen, L. Wang, W. Cai, Journal of Catalysis 115967(2025); https://doi.org/10.1016/j.jcat.2025.115967
[39] M. Honarmand, M. Golmohammadi, J. Hafezi-Bakhtiari, Environmental Science and Pollution Research 28 7123-7133(2021); https://doi.org/10.1007/s11356-020-11086-3
[40] D. Bekchanov, M. Mukhamediev, A. Inkhonova, D. Eshtursunov, G. Babojonova, O. Rajabov, U. Khalilov, M. Yusupov, P. Lieberzeit, Environmental Research 120911(2025); https://doi.org/10.1016/j.envres.2025.120911
[41] M. Bashar, S. Sobhanardakani, M. Cheraghi, B. Lorestani, B. Shahmoradi, Water, Air, and Soil Pollution 236 154(2025); https://doi.org/10.1007/s11270-025-07790-w
[42] T.A. Kurniawan, Z. Mengting, D. Fu, S. K. Yeap, M. H. D. Othman, R. Avtar, T. Ouyang, Journal of Environmental Management 270 110871(2020); https://doi.org/10.1016/j.jenvman.2020.110871

[43] Z.A. Khan, S.A. Naqvi, A. Mukhtar, Z. Hussain, S.A. Shahzad, A. Mansha, M. Ahmad, A.F. Zahoor, I.H. Bukhari, M.R. Ashraf-Janjua, N. Mahmood, M. Yar, Pakistan Journal of Pharmaceutical Sciences 27 469-474(2014); https://doi.org/10.2139/pps.5243661
[44] A. Azizi, P. Amiri, P. A. Roozbahani, M. Shariati, Nanotechnology for Environmental Engineering 10 1-18(2025); https://doi.org/10.1007/s41204-025-00426-8
[45] Y. Raza, H. Raza, A. Ahmed, M. M. Quazi,M. Jamshaid, M. T. Anwar, M. N. Bashir, T. Younas, A. T. Jafry, M. E. M. Soudagar, Polymer Composites (2025); https://doi.org/10.1002/pc.30011